Electronic supplementary information:

Sacrificial agent-free photocatalytic H_2O_2 evolution via two-electron oxygen reduction using a ternary α-Fe_2O_3/CQD@g-C_3N_4 photocatalyst with broad-spectrum response

Xi Chen [a, b], Wenwen Zhang [b], Lixiang Zhang [c, b], Luping Feng [a, b], Chunxian Zhang [b], Jie Jiang [d], Tingjiang Yan[b], Hua Wang [a, b, d*]

[a] School of Chemistry and Chemical Engineering, Harbin Institute of Technology, Harbin, Heilongjiang 150090, P. R. China.

[b] Institute of Medicine and Materials Applied Technologies, College of Chemistry and Chemical Engineering, Qufu Normal University, Qufu, Shandong 273165, P. R. China.

[c] School of Environment, Harbin Institute of Technology, Harbin, Heilongjiang 150090, P. R. China.

[d] School of Marine Science and Technology, Harbin Institute of Technology at Weihai, Weihai, Shandong 264209, P. R. China.

*Corresponding Author: E-mail addresses: huawang@qfnu.edu.cn; Tel: +86 537 4456306; Web: http://wang.qfnu.edu.cn.

Experimental Section

Synthesis of carbon quantum dots (CQDs). The CQDs were prepared from the decomposition of isopropanol via a solvothermal method. Typically, 16.4 mL IPA was added into 13.6 mL DMF. The mixture was then autoclaved in a 70 mL Teflon container at 180°C for 8 h. After cooling to room temperature, the CQDs solution was obtained in the end.

Synthesis of α-Fe_2O_3@g-C_3N_4. Typically, an aliquot of 0.10 g of ultrathin g-C_3N_4 and 13.6 mL of α-Fe_2O_3 precursor solution above was introduced into 16.4 mL DMF under vigorous stirring. After the ultrasonic dispersion for 30 min, the mixture was transferred into a 70 mL Teflon-lined autoclave, and heated at 180°C for 8 h. Afterwards, the α-Fe_2O_3@g-C_3N_4 was collected by centrifugation and washed for three times with ethanol, followed by being dried at 60°C overnight.

Characterization of Photocatalytic Materials

X-ray diffraction (XRD) measurements were performed using a powder diffractometer (Rjgaku/MiniFlex600) in the 2θ range of 10° - 80° with a Cu Kα radiation. X-ray photoelectron spectra (XPS) were recorded by a spectrometer (ESCALAB 250Xi) using Al Kα radiation with the C 1s peak (284.6 eV) as reference. The microstructures of the samples were explored by the transmission electron microscopy (TEM, JEOL/JEM-2100PLUS) with electron energy of 15 kV. The UV–vis diffuse reflection spectra (DRS) of samples were measured with the spectrophotometer (Shimadzu/UV-3600) using $BaSO_4$ as reference in the range of 360 - 800 nm. Electron spin resonance (ESR) tests of samples were conducted using a spectrometer (JEOL/JES-FA200) to prove the presence of $\cdot O_2^-$ in the photocatalysis reactions.

Electrochemical Tests

Rotating ring-disk electrode (RRDE) and rotating disk electrode (RDE) measurements were accomplished through an electrochemical workstation (Chenhua CHI 760E) with a four-electrode system (Pine/AFMSRCE). The working electrode was prepared as follows: 5 mg of the product was dispersed into 1 mL of mixed solution containing 475 μL ethanol, 475 μL water, and 50 μL Nafion. Subsequently, 10 μL of this suspension was dropped on a glassy carbon electrode, followed by air drying at 80 °C. The ring-disk electrode was included a glassy carbon disk

(0.2475 cm^2) and a Pt ring (0.1866 cm^2). The Pt ring potential was sustained at 1.48 V (*vs.* RHE). The Ag/AgCl electrode and Pt wire electrode were respectively employed as the reference electrode and counter electrode. The linear sweep voltammetry (LSV) curves were acquired in an O_2-saturated 0.10 M PBS solution after N_2 and O_2 bubbling for 30 min (pH 7.0). Besides, the electrochemical workstation was also conducted for the Mott-Schottky curves, electrochemical impedance spectroscopy, and transient photocurrent responses of different samples using conventional three-electrode system. Herein, the working electrode was fabricated by dip-coating a 5.0 μL of sample slurry (5 mg/mL aqueous Nafion) on glassy carbon electrode (3 mm^2) and dried at room temperature.

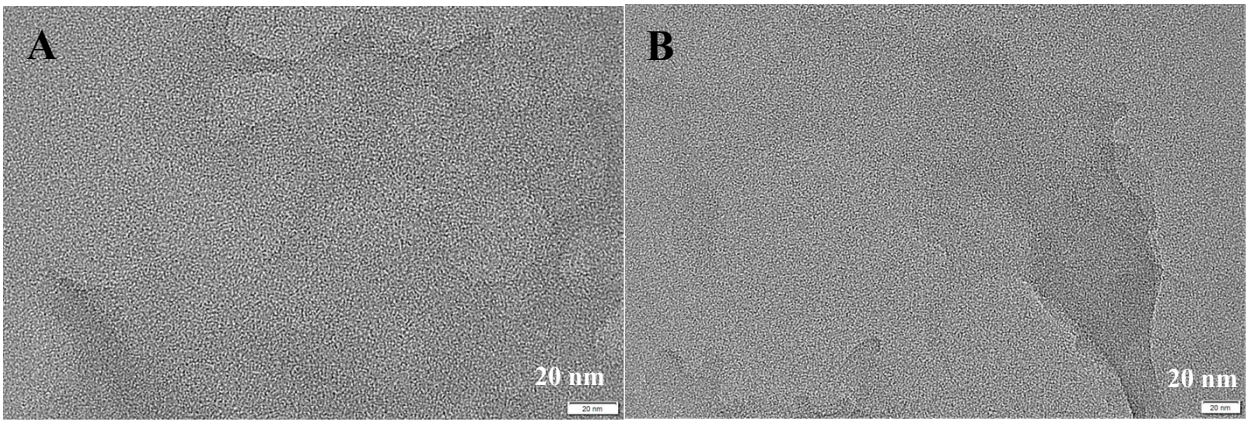

Fig. S1. HRTEM images of (A) ultrathin g-C_3N_4 with (B) different amplified parts.

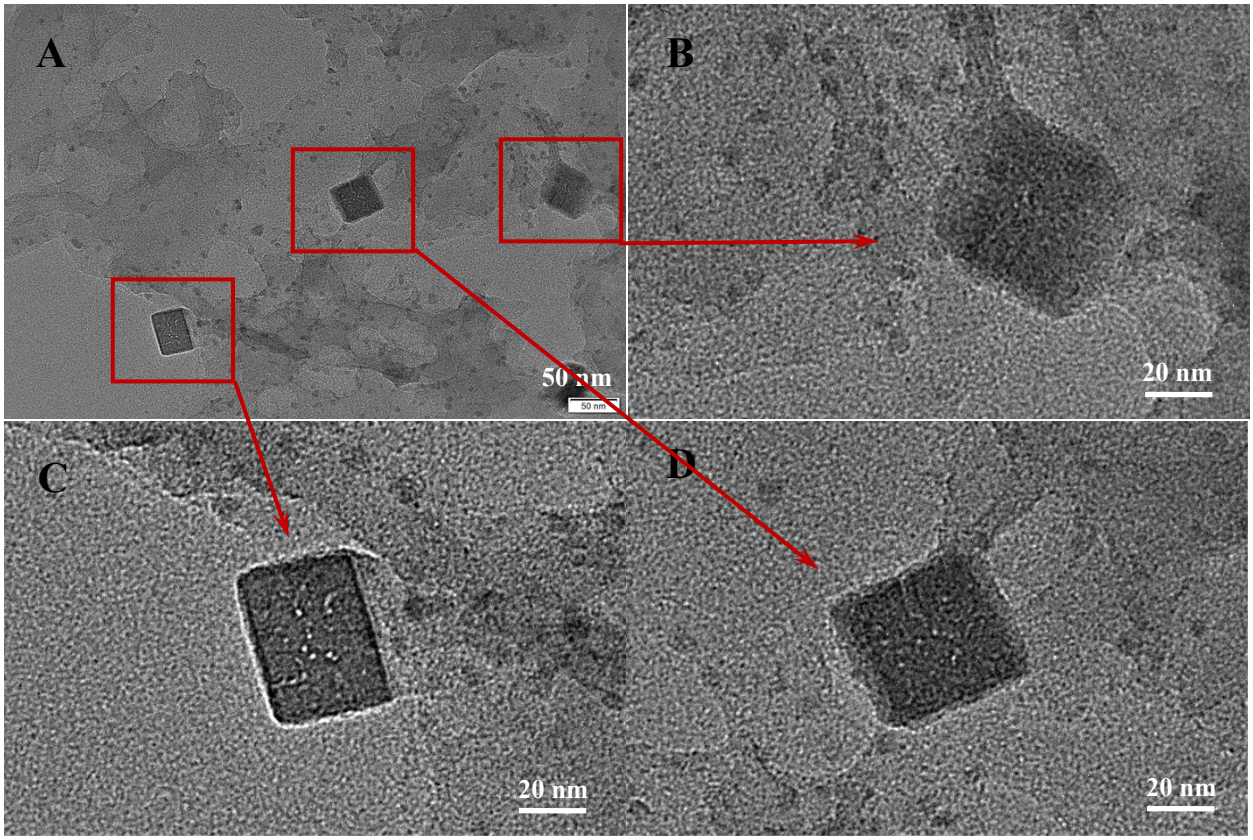

Fig. S2. TEM images of α-Fe_2O_3/CQD@g-C_3N_4 of (A) full, with (B-D) different magnification-amplified parts.

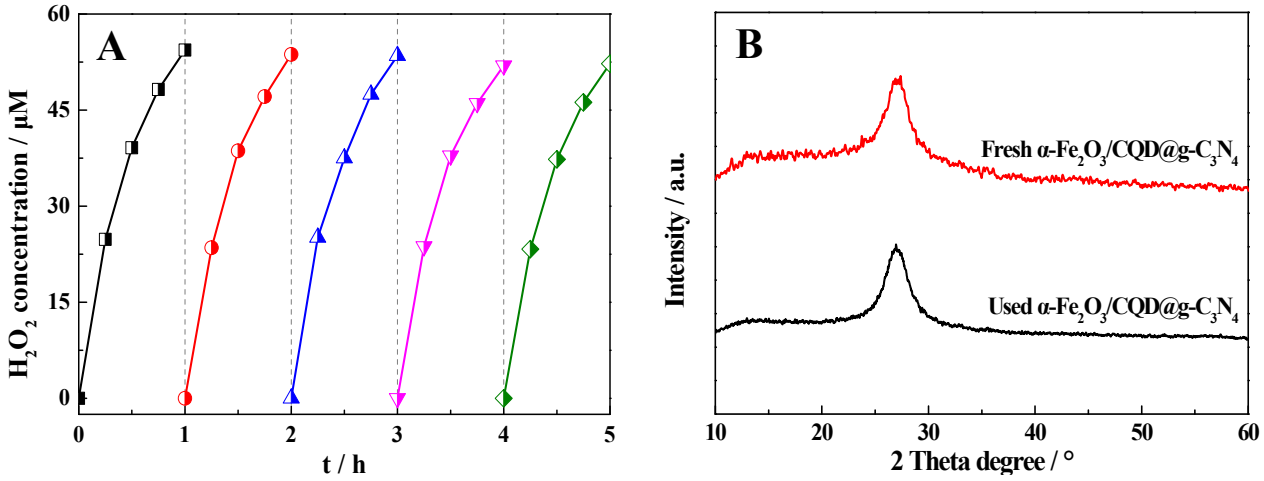

Fig. S3. (A) The stability test results of α-Fe_2O_3/CQD@g-C_3N_4 for five runs in O_2-equilibrated water; (B) XRD patterns of α-Fe_2O_3/CQD@g-C_3N_4 before and after five runs.

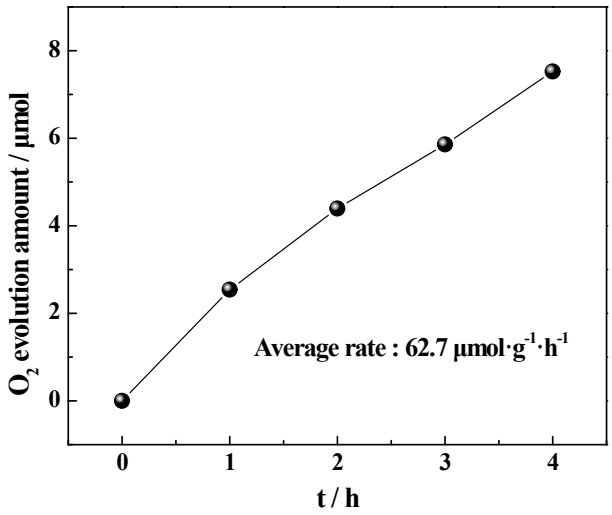

Fig. S4. The results of α-Fe_2O_3/CQD@g-C_3N_4-photocatalyzed O_2 evolution under visible light irradiation using 1.0 mM of $AgNO_3$ as the photoelectron quencher. The experiments were carried out in a Labsolar-6A photocatalytic system under vacuum condition with the reaction solutions (pH 7.0) containing 30 mL H_2O and 30 mg photocatalyst.

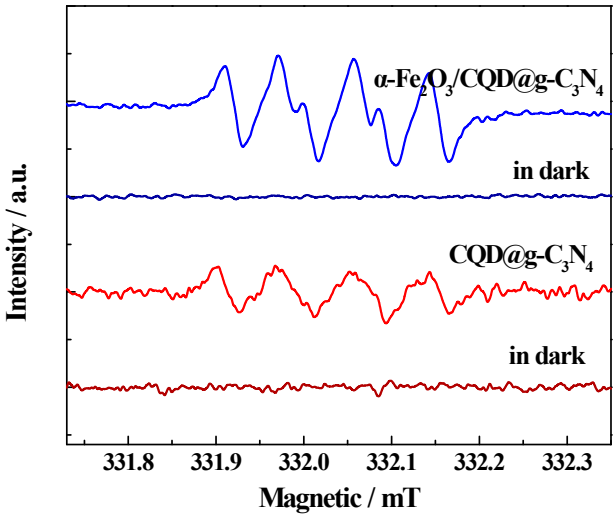

Fig. S5. DMPO-·O_2^- spin-trapping ESR spectra of α-Fe_2O_3/CQD@g-C_3N_4 and CQD@g-C_3N_4 in the photo-degradation of methanol before and after 5 min visible light illumination.

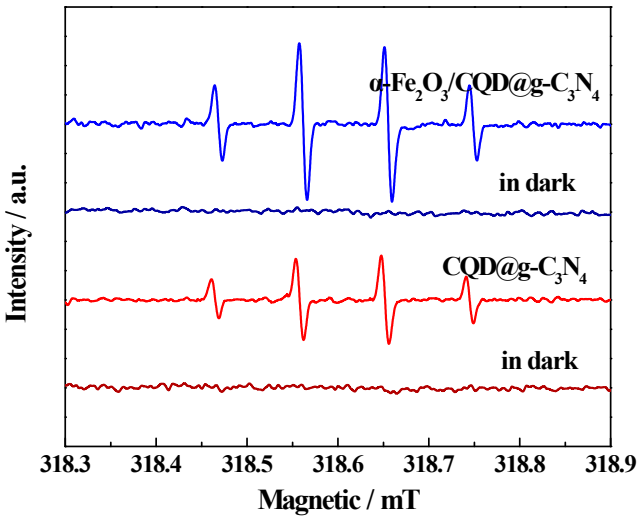

Fig. S6. DMPO-·OH spin-trapping ESR spectra of CQD@g-C_3N_4 and α-Fe_2O_3/CQD@g-C_3N_4 in water before and after 10 min illumination.

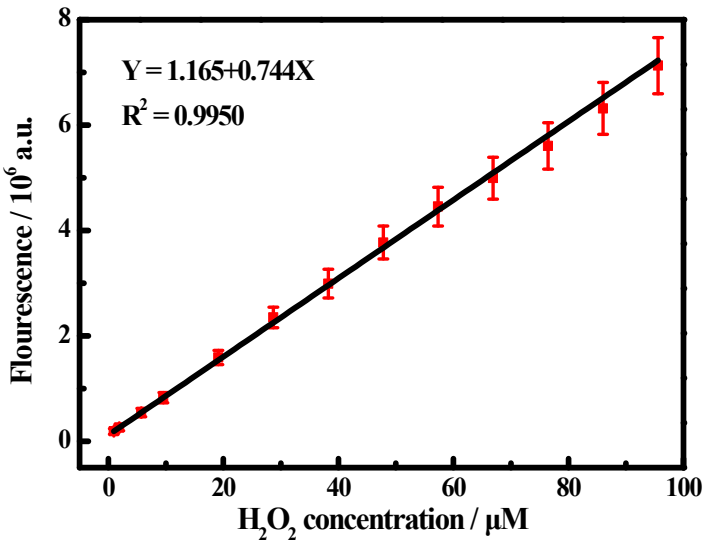

Fig. S7. The calibration curve of fluorescence intensities versus different H_2O_2 concentrations.

Table S1. Element content analysis of α-Fe_2O_3/CQD@g-C_3N_4 composite from XPS spectra (Atomic %)

Sample	C/%	N/%	Fe/%	O/%
α-Fe_2O_3/CQD/g-C_3N_4	50.18	40.24	2.82	6.76

Table S2. Energy band gaps, conduction band potentials, and valence band potentials of ultrathin g-C_3N_4 and (110) exposed α-Fe_2O_3.

Samples	E_g/eV	E_{CB}/eV	E_{VB}/eV
ultrathin g-C_3N_4	2.81	-1.13	1.68
(110) exposed α-Fe_2O_3	2.17	0.26	2.43

Table S3. Comparison of photocatalytic performances for H_2O_2 production among different photocatalysts.

Photocatalyst	Cocatalyst	Sacrificial agent	Gas atmosphere (air)	Materials input (mg)	H_2O_2 yield rate ($\mu mol \cdot g^{-1} \cdot h^{-1}$)	Ref.
g-C_3N_4/PWO	/	/	/	100	29	[1]
Cv/g-C_3N_4	/	/	/	100	ca. 92	[2]
g-C_3N_4/CoWO	/	/	/	100	187	[3]
$Cu_2(OH)PO_4$/g-C_3N_4	/	/	saturated O_2	200	400	[4]
mesoporous g-C_3N_4	/	C_2H_6O	saturated O_2	20	ca. 187.5	[5]
SN-GQD/TiO_2	/	C_3H_8O	saturated O_2	25	110.4	[6]
rGO/$Cd_3(TMT)_2$	/	CH_3OH	/	80	95	[7]
g-C_3N_4/CNTs	/	HCOOH	/	100	326	[8]
APTMS/TiO_2	Pd	phosphate	/	5	300	[9]
TiO_2	Au/Ag	C_2H_6O	saturated O_2	5	150	[10]
α-Fe_2O_3/CQD@g-C_3N_4	**/**	**/**	saturated O_2	**5**	**138.6**	**This work**

References

[1] S. Zhao and X. Zhao, Polyoxometalates-derived metal oxides incorporated into graphitic carbon nitride framework for photocatalytic hydrogen peroxide production under visible light, *J. Catal.*, 2018, **366**, 98-106.

[2] S. Li, *et al*. Effective photocatalytic H_2O_2 production under visible light irradiation at g-C_3N_4 modulated by carbon vacancies, *Appl. Catal. B-Environ.*, 2016, **190**, 26-35.

[3] S. Zhao and X. Zhao, Insights into the role of singlet oxygen in the photocatalytic hydrogen peroxide production over polyoxometalates-derived metal oxides incorporated into graphitic carbon nitride framework, *Appl. Catal. B-Environ*., 2019, **250**, 408-418.

[4] X. Wang, Z. Han, L. Yu, C. Liu, Y. Liu and G. Wu, Synthesis of full-spectrum-response $Cu_2(OH)PO_4$/g-C_3N_4 photocatalyst with outstanding photocatalytic H_2O_2 production performance via a "Two Channel Route", *ACS Sustain. Chem. Eng.*, 2018, **6**, 14542-14553.

[5] Y. Shiraishi, Y. Kofuji, H. Sakamoto, S. Tanaka, S. Ichikawa and T. Hirai, Effects of surface defects on photocatalytic H_2O_2 production by mesoporous graphitic carbon nitride under visible light irradiation, *ACS Catal.*, 2015, **5**, 3058-3066.

[6] L. Zheng, *et al.* Highly selective photocatalytic production of H_2O_2 on sulfur and nitrogen co-doped graphene quantum dots tuned TiO_2, *Appl. Catal. B-Environ*., 2018, **239**, 475-484.

[7] J. Xu, *et al.* $Cd_3(C_3N_3S_3)_2$ coordination polymer/graphene nanoarchitectures for enhanced photocatalytic H_2O_2 production under visible light, *Sci. Bull.*, 2017, **62**, 610-618.

[8] S. Zhao, T. Guo, X. Li, T. Xue, B. Yang and X. Zhao, Carbon nanotubes covalent combined with graphitic carbon nitride for photocatalytic hydrogen peroxide production under visible light, *Appl. Catal. B-Environ.*, 2018, **224**, 725-732.

[9] C. Chu, *et al.* Electronic tuning of metal nanoparticles for highly efficient photocatalytic hydrogen peroxide production, *ACS Catal.*, 2019, **9**, 626-631.

[10] D. Tsukamoto, *et al.* Photocatalytic H_2O_2 production from ethanol/O_2 system using TiO_2 loaded with Au-Ag bimetallic alloy nanoparticles, *ACS Catal.*, 2012, **2**, 599-603.